DFT Calculations and Thermodynamic Re-Assessment of the Fe-Y Binary System

Ling Fan[1] · Chen Shen[2] · Kun Hu[3] · Huashan Liu[3] · Hongbin Zhang[2]

Abstract Based on the CALPHAD method combined with density functional theory (DFT) calculations, we performed a thermodynamic reassessment of the binary Fe-Y system leading to good agreement with the available experimental measurements. The electronic, vibrational, and magnetic contributions to the specific heat and thus the Gibbs free energy were evaluated based on accurate DFT calculations for the Fe-Y intermetallic compounds. Moreover, a new model was applied to describe the Gibbs free energies of such intermetallic phases which leads to significant improvements over the conventional thermodynamic expressions. The resulting phase diagram and thermodynamic properties are in good consistency with the previous experimental data, paving the way to designing multicomponent magnetic functional materials.

Keywords Fe-Y binary system · DFT calculation · CALPHAD method

✉ Chen Shen
chenshen@tmm.tu-darmstadt.de

✉ Hongbin Zhang
hzhang@tmm.tu-darmstadt.de

1   Institute of Applied Materials (IAM-CMS), Karlsruhe Institute of Technology (KIT), 76131 Karlsruhe, Germany

2   Institute of Materials Science, Technical University of Darmstadt, 64287 Darmstadt, Germany

3   School of Materials Science and Engineering, Central South University, Changsha 410083, China

1 Introduction

Permanent magnets have a vast spectrum of applications on energy harvesting and conversion, thus there is a strong impetus to engineer novel permanent magnet materials.[1] Nd-Fe-B based magnets have been established as prototypical high-performance permanent magnets since their discovery in the 1980s.[2] Given Nd as one of the critical elements whose price is subject to strong fluctuations, it is an interesting question whether substitutional elements can be applied to design permanent magnets with comparable or enhanced performance. From the chemistry point of view, Yttrium exhibits similar properties as the lanthanide elements. As the abundance of Y in the earth's crust is higher than all the other rare earth elements except Ce, the substitution of Y for Nd has attracted intensive attention recently.[3] For instance, materials like Fe-Nd-Y-B[3] and Fe-Nd-Ce-Y-B[4] have been investigated. In this regard, a comprehensive description of the thermochemistry and phase equilibria of the Y-Fe subsystem is critical for further systematic processing of the Fe-(Nd,Y)-B-based materials. E.g, based on the current thermodynamic assessment of the Nd-Fe-B phase diagram, an optimization of the quaternary Fe-Nd-Y-B phase diagram can be carried out using the CALPHAD method after evaluating the thermodynamic properties of the Y-Fe, Y-Nd, Y-B, and the relevant ternary cases.

Despite there have been several thermodynamic assessments reported on the Fe-Y system,[5-7] the current Fe-Y phase diagram is still not consistent, which can be attributed to the lack of systematic experimental measurements for sufficient thermodynamic data. On the other hand, density functional theory (DFT) calculations have been demonstrated to be a reliable way to provide the missing thermochemical information, which have been

successfully applied on the Zn-Ti,[8] Yb-Ni,[9] and Re-Y[10] systems.

In this work, we performed DFT calculations to obtain the finite temperature thermodynamic properties of the Fe-Y intermetallic phases, including the enthalpy of formation, entropy, Gibbs energy and heat capacity. Combined with the CALPHAD method, we established a new thermodynamic model to parameterize the Gibbs energies of the intermetallic compounds. Correspondingly, the Fe-Y binary phase diagram is re-assessed combining the DFT calculations, CALPHAD modelling, and the available experiments, leading to a consistent thermodynamic description. This paves the way to systematically re-assess the thermodynamic phase diagrams of the constitute binary and ternary systems which are indispensable for designing multicomponent materials.

2 Literature Review

2.1 Phase Diagram

Based on the x-ray diffraction(XRD) and metallographic results, Domagala et al.[11] firstly studied the Fe-Y phase diagram over the whole composition range, with two follow-up assessments done by Gschneider et al.[12] and Kubaschewski et al.[13] Both optimizations accepted the basic phase diagram proposed by Domagala et al.[11] Nevertheless, Gschneider et al.[12] pointed out that the Liquidus, obtained by Domagala et al.,[11] was unjustified. Additionally, Kubaschewski[13] made minor revisions on the phase stoichiometries so that the results became consistent with crystallographic studies. The most recent experimental investigation was performed by Zhang et al.,[14] focusing mostly on the crystal structures as well

Fig. 1 The experimental phase diagram of the Fe-Y binary system[13]

as the magnetic and thermodynamic properties, but not the phase relations.

Figure 1 shows the Fe-Y phase diagram obtained by Kubaschewski,[13] where four intermetallic compounds, i.e., $Fe_{17}Y_2$, $Fe_{23}Y_6$, Fe_3Y and Fe_2Y, can be identified. Among them, the $Fe_{23}Y_6$ and Fe_2Y phases are thought to have homogeneity ranges. However, there is no further experimental report on the solubility range of the $Fe_{23}Y_6$ phase. According to Domagala et al. three phases, i.e., $Fe_{17}Y_2$, $Fe_{23}Y_6$ and Fe_3Y, melt congruently. However, the congruent temperature for the $Fe_{23}Y_6$ and Fe_3Y phases is not clear, and the melting point of $Fe_{17}Y_2$ is simply estimated in Ref. [11]. Buschow[15] reported that the $Fe_{17}Y_2$ phase should have a dimorphic structure with the high (low) temperature structure being the $Ni_{17}Th_2(Zn_{17}Th_2)$-type, respectively. Nevertheless, since the allotropy transformation temperature between the high-temperature and low-temperature $Fe_{17}Y_2$ is not determined, we considered only the lower-temperature $Zn_{17}Th_2$-type phase in this work. The crystalline data of all solid phases are listed in Table 1.

In the Fe–Y binary system, the solubility of Y in Fe is very low (less than 0.1 at.%) and that of Fe in Y is about 2–3 at.% at 1173 K.[13] It was also found that the invariant reactions involved in the intermetallic compounds are three eutectic reactions, (1) liquid → γFe + $Fe_{17}Y_2$; (2) liquid → $Fe_{17}Y_2$ + $Fe_{23}Y_6$; (3) liquid → $Fe_{23}Y_6$ + Fe_3Y, and one peritectic reaction with the formation of Fe_2Y through Liquid + Fe_3Y → Fe_2Y.[13] Table 2 summarises the experimental data of the phase equilibrium and invariant reactions in the Fe-Y system.

2.2 Thermochemical Properties

Ryss et al.[23] measured the enthalpies of mixing (H_{mix}) of the liquid phase at 1873 K in the entire composition range with an interval of 5 at.%. The results show a minimum of integral enthalpy, about − 8.44 kJ/mol at 47 at.% Y. The activity of Y and Fe in the Fe-Y system was determined by Nagai et al.[24] using the multi-Knudsen cell mass spectrometry method, with the pure Y (HCP) and Fe (FCC) as the references. Interestingly, the activity of Y showed a large negative deviation from the ideal solution behavior on the Y rich side.

The enthalpies of formation for four intermetallic compounds at 298 K ($\Delta H_{f,298}$) were predicted to be − 2 kJ/mol-atom by Van Mal et al.,[25] based on the theory of Miedema[26]. Gozzi et al.[27] reported a $\Delta H_{f,298}$ of − 8.7 kJ/mol-atom for the $Fe_{17}Y_2$ phase, which was evaluated too negative by Konar et al.[7] when comparing to the other Fe-rare-earth(RE) binary systems. The only experimental investigation on $\Delta H_{f,973}$ of $Fe_{17}Y_2$, $Fe_{23}Y_6$, Fe_3Y, and
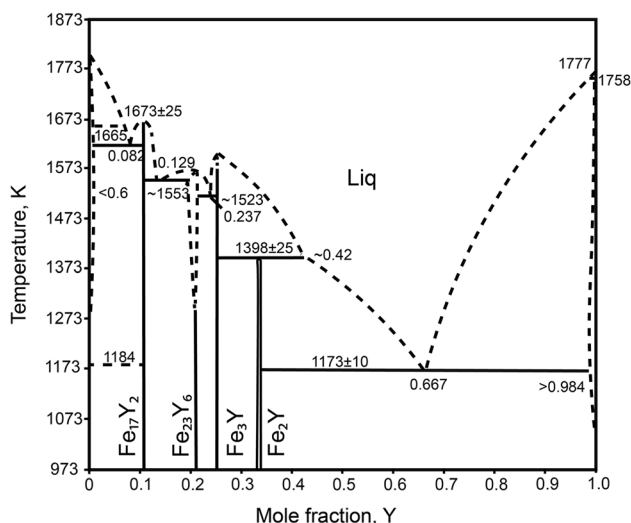
Table 1 The crystal structures of the elementary and intermetallic phases of Fe-Y in comparison with previous experimental (EXP) studies and calculations (Calc)

Phase	Space group	Prototype	Person symbol	Lattice parameters(Å)		Refs.
				a	c	
αFe	$Im\bar{3}m$	W	cI2	2.833	…	This work
				2.842	…	Exp[16]
				2.802	…	Calc[17]
γFe	$Fm\bar{3}m$	Cu	cF4	3.660	…	Exp[18]
δFe	$Im\bar{3}m$	W	cI2	2.932	…	Exp[19]
αY	P63/mmc	Mg	hp2	3.659	5.678	This work
				3.652	5.711	Exp[20]
				3.656	5.679	Calc[10]
$Fe_{17}Y_2$	$R\bar{3}m$	$Zn_{17}Th_2$	hR57	8.447	12.386	This work
				8.460	12.410	Exp[21]
$Fe_{23}Y_6$	$Fm\bar{3}m$	$Mn_{23}Th_6$	cF116	12.040	…	This work
				12.120	…	Exp[21]
Fe_3Y	$R\bar{3}m$	Ni_3Pu	hR36	5.111	24.280	This work
				5.095	24.390	Exp[21]
Fe_2Y	$Fd\bar{3}m$	Cu_2Mg	cF24	7.280	…	This work
				7.363	…	Exp[21]
				7.280	…	Calc[22]

Fe_2Y was preformed by Subramanian and Smith,[28] by using the solid electrolyte cells Electro Motive Force (EMF) method (Table 3). DFT calculations on the enthalpies of formation for the Fe-Y systems were carried out by Mihalkovic and Widom,[29] predicting Fe_3Y and Fe_2Y being stable while $Fe_{17}Y_2$ and $Fe_{23}Y_6$ metastable at low temperature. The enthalpies of formation obtained by the experiments and DFT calculations at different temperatures are listed in Table 3.

The only measurement on the heat capacity of the Fe-Y systems was done for $Fe_{17}Y_2$ by Mandal et al.[32]. It is noted that Mandal et al.[32] obtained the heat capacity of $Fe_{17}Y_2$ at a constant pressure in the temperature range of 2–300 K. However, the XRD patterns for their samples showed a strong deviation from the literature,[15] thus such data are not used in this work.

2.3 Magnetic Properties

The Curie temperature (T_c) and magnetic moments of the intermetallic Fe-Y compounds have been experimentally and theoretically investigated, as summarized in Table 4. Such quantities are critical to evaluate the magnetic contribution to the Gibbs free energy and heat capacity, as discussed later in detail.

2.4 Previous Assessments

Scarcity of the experimental data makes an accurate thermodynamic optimization of the Fe-Y system challenging,

though there are several reports in the literature. The Fe-Y phase diagram was firstly assessed by Du et al.,[38] with a few inconsistencies between the experimental and calculated data on the phase relations as well as the thermodynamic properties. For instance, $Fe_{23}Y_6$ would form following a peritectic reaction Liquid + $Fe_3Y \rightarrow Fe_{23}Y_6$ at 1573 K, which is obviously contradictory to the experiments done in Ref.[11]. Later, the Fe-Y phase diagram was reported in Ref.[39, 40]. However, neither the thermodynamic parameters of the liquid and solid phases nor the information of the invariant reactions were given, making it difficult to justify their assessments.

Kardellass et al.[5] re-assessed the Fe-Y system using two methods (polynomial temperature dependence (PTD) and exponential temperature dependence (ETD)) to model the excess Gibbs energy of the Liquid phase. As the miscibility gap was given in the liquid phase at low temperature, it is observed that both thermodynamic descriptions cause artefacts in the high-order systems. Seanko et al.[6] and Konar et al.[7] published their thermodynamic data on the Fe-Y binary system in the same year. Both studies did not reproduce the phase diagram better than the previous work. Besides, the thermodynamic properties, such as the activity from 1473 to 1573 K and the mixing enthalpy of Liquid at 1873 K, have not been significantly improved in Ref.[6, 7] when compared with the previous assessments. Therefore, further investigation on the thermodynamics of the Fe-Y system is necessary.

Table 2 Summary of the experimental (Exp) and optimized (Opt) invariant reactions in the Fe-Y system

Phase	Type	T/K	Phase composition (Y,at.%)			Refs.
L+δFe → γFe	Peritectic	1673±25	…	…	…	Exp[13]
		1660	6.00	…	…	This work
		1665	7.19	…	…	Opt[6]
		1725	3.90	…	…	Opt[7]
		1664	4.79	…	…	Opt[5]
		1663	4.79	…	…	Opt[5]
L → γFe + Fe$_{17}$Y$_2$	Eutectic	1623 ± 25	8.20	< 0.60	10.50	Exp[13]
		1635	7.00	…	10.50	This work
		1641	8.40	0.10	10.50	Opt[6]
		1659	6.90	…	10.50	Opt[7]
L → δFe + Fe$_{17}$Y$_2$	Eutectic	1663	7.19	…	10.50	Opt 5]
γFe → αFe + Fe$_{17}$Y$_2$	Eutectoid	1185	…	…	10.50	Exp[13]
		1185	…	…	10.50	This work
		1185	…	…	10.50	Opt[6]
		1185	…	…	10.50	Opt[5]
		1185	…	…	10.50	Opt[5]
L → Fe$_{23}$Y$_6$ + Fe$_{17}$Y$_2$	Eutectic	∼1553	12.90	…	10.50	Exp[13]
		1613	17.30	20.69	10.50	This work
		1605	19.74	20.70	10.50	Opt[6]
		1638	17.90	…	10.50	Opt[5]
		1605	18.15	…	10.50	Opt[5]
		1645	15.90	…	10.50	Opt[7]
L → Fe$_{23}$Y$_6$+Fe$_3$Y	Eutectic	∼ 1523	23.70	20.69	25.00	Exp[13]
		1619	20.69	20.69	25.00	This work
		1604	23.36	20.50	25.00	Opt[6]
		1640	21.63	…	25.00	Opt[5]
		1605	20.69	…	25.00	Opt[5]
		1667	21.00	…	25.00	Opt[7]
L+Fe$_3$Y → Fe$_2$Y	Peritectic	1398 ± 25	42.40	25.00	33.30	Exp[13]
		1416	46.70	25.00	33.30	This work
		1396	52.48	25.00	33.54	Opt[6]
		1394	48.20	25.00	33.30	Opt[5]
		1409	44.30	25.00	33.30	Opt[5]
		1397	47.50	25.00	33.30	Opt[7]
L → Fe$_2$Y+αY	Eutectic	1173	66.00	…	98.40	Exp[13]
		1128	64.00	33.30	…	This work
		1201	66.09	33.70	99.20	Opt[6]
		1118	63.70	…	…	Opt[5]
		1146	61.20	…	…	Opt[5]
		1156	60.10	…	…	Opt[7]
βY → αY+L	Peritectic	1751	…	…	…	Exp[13]
		1756	99.74	98.26	99.73	Opt[6]
		1749	…	…	97.60	Opt[5]
		1750	…	…	97.90	Opt[5]
βY+L → αY	Eutectic	1756	99.74	98.26	99.73	Opt[7]
		1754	99.95	98.00	99.90	This work
L → Fe$_{17}$Y$_2$	Congruent	1673 ± 25	10.50	…	…	Exp[13]
		1650	10.50	…	…	This work

Table 2 continued

Phase	Type	T/K	Phase composition (Y,at.%)			Refs.
		1644	10.50	…	…	Opt[6]
		1672	10.50	…	…	Opt[5]
		1676	10.50	…	…	Opt[5]
		1679	10.50	…	…	Opt[7]
L → Fe$_{23}$Y$_6$	Congruent	…	…	…	…	Exp[13]
		1623	20.69	…	…	This work
		1641	20.05	…	…	Opt[5]
		1606	20.75	…	…	Opt[5]
		1606	20.75	…	…	Opt[6]
		1667	20.70	…	…	Opt[7]
L → Fe$_3$Y	Congruent	…	25.00	…	…	Exp[13]
		1621	25.00	…	…	This work
		1647	25.00	…	…	Opt[5]
		1623	25.00	…	…	Opt[5]
		1605	25.00	…	…	Opt[6]
		1681	25.00	…	…	Opt[7]

Table 3 The enthalpies of formation at different temperatures ($\Delta H_{f,0}$, $\Delta H_{f,298}$, $\Delta H_{f,973}$) of the Fe-Y systems from DFT calculations (DFT), CALPHAD-modeling (Opt), and experimental (Exp) measurements

Phase	$\Delta H_{f,0}$ kJ/mol-at	Method	Refs.	$\Delta H_{f,298}$ kJ/mol-at	$\Delta H_{f,973}$ kJ/mol-at	Method	Refs.
Fe$_{17}$Y$_2$	− 1.040	DFT	This work	− 2.287	− 5.691	Opt	This work
	− 1.056	DFT	30	…	− 6.380 ± 0.31	Exp	28
	− 2.672	DFT	31	− 4.360	− 7.770	Opt	6
	− 1.634	DFT	29	− 5.990	− 9.470	Opt	5
	…	-	…	− 5.290	− 8.760	Opt	5
Fe$_{23}$Y$_6$	− 4.089	DFT	This work	− 5.752	− 6.523	Opt	This work
	− 4.031	DFT	31	…	− 8.090 ± 0.49	Exp	28
	− 4.416	DFT	30	− 6.250	− 9.220	Opt	6
	− 4.829	DFT	29	− 12.050	− 11.690	Exp	5
	…	…	…	− 12.970	− 12.650	Opt	5
Fe$_3$Y	− 6.06	DFT	This work	− 6.374	− 6.774	Opt	This work
	− 6.144	DFT	31	…	− 8.970 ± 0.54	Exp	28
	− 6.144	DFT	30	− 6.960	− 8.940	Opt	6
	− 7.519	DFT	29	− 13.040	− 12.490	Opt	5
	…	…	…	− 13.310	− 12.770	Opt	5
Fe$_2$Y	− 5.920	DFT	This work	− 6.412	− 6.825	Opt	This work
	− 6.048	DFT	31	…	− 7.090 ± 0.61	Exp	28
	− 6.240	DFT	30	− 6.300	− 7.770	Opt	6
	− 7.646	DFT	29	− 9.990	− 12.550	Opt	5
	…	…	…	− 12.470	− 11.800	Opt	5

Table 4 The Curie temperature (T_c) and mean magnetic moment of the intermetallic Fe-Y compounds, obtained based on DFT calculations (DFT) and experimental (Exp) measurements

Phase	T_c (K)	Magnetic moment (μ_B per Fe atom)	Magnetic property	Refs.
$Fe_{17}Y_2$	…	2.30	FM	This work
	328	2.20	FM	Exp[33]
$Fe_{23}Y_6$	…	2.20	FM	This work
	…	1.79	FM	DFT[34]
	484	1.86	FM	Exp[35]
Fe_3Y	…	1.92	FM	This work
	…	1.52	FM	DFT[34]
	569	1.75	FM	Exp[36]
Fe_2Y	…	1.62	FM	This work
	…	1.36	FM	DFT[34]
	545	1.54	FM	Exp[37]

3 Methodology

3.1 DFT calculations on the thermodynamic properties at finite temperatures

Assuming the electronic, vibrational, and magnetic degrees of freedom are independent due to the orders of magnitude difference in the time scale for the corresponding excitations, the Gibbs free energy $G(T, P)$ at temperature T and pressure P can be obtained from the Helmholtz free energy $F(T, V)$ as follows:[9]

$$G(P,T) - PV = F(T,V) = E_0(V) + F_{vib}(V,T) + F_{el}(V,T) + F_{magn}(V,T).$$
(Eq 1)

The first term, $E_0(V)$ in Eq 1, is the total energy at zero Kelvin without the zero-point energy contribution, which can be obtained by fitting of the energy versus volume data using the Brich-Murnaghan equation of state (EOS):[41]

$$E_0(V) = a + bV^{-2/3} + cV^{-3/4} + dV^{-2},$$
(Eq 2)

where a, b, c and d are the fitting parameters. The minimum value of EOS at 0 K is the 0 K static energy at the equilibrium volume (V_0).

The second term F_{vib} accounts for the contribution of the lattice vibrations to the Helmholtz energy, which can be derived from the phonon density of states (PhDOS), $g(\omega, V)$, by using the following equation:[9]

$$F_{vib}(V,T) = k_B T \int_0^\infty \ln\left[2\sinh\frac{\hbar\omega}{2k_B T}\right] g(\omega,V)d\omega,$$
(Eq 3)

where k_B and $\hbar$ are the Boltzmann constant and reduced Planck constant, respectively, and ω denotes the phonon frequency for a given wave vector q. The PhDOS $g(\omega, V)$ can be obtained by integrating the phonon dispersion in the Brillouin zone.

The third term F_{el} represents the electronic contribution to the Helmholtz energy, obtained by [8]:

$$F_{el}(V,T) = E_{el}(V,T) - T \cdot S_{el}(V,T)$$
(Eq 4)

where $E_{el}(V,T)$ and $S_{el}(V,T)$ indicate the electronic energy and electronic entropy, respectively. With the electronic DOS, both terms can be formulated as [8]:

$$E_{el}(V,T) = \int n(\epsilon)f\epsilon d\epsilon - \int_{-\infty}^{\epsilon_F} n(\epsilon,V)d\epsilon,$$
(Eq 5)

$$S_{el}(V,T) = -k_B \int n\epsilon[f\ln f + (1-f)\ln(1-f)]d\epsilon,$$
(Eq 6)

where $n(\epsilon)$ is the electronic DOS, f represents the Fermi-Dirac distribution function and ϵ_F is the Fermi energy.

The last term in Eq 1 is the magnetic contribution to the Gibbs energy. Based on the Inden-model,[42] the magnetic Gibbs energy can be formulated as:

$$G^{magn} = RT\ln(\beta^\varphi + 1)f(\tau), \tau = T/T_c^\varphi,$$
(Eq 7)

where T_c^φ is the T_C for the phase-φ. β^φ is the average magnetic moment per atom. In addition, $f(\tau)$ represents a polynomial obtained by Hillert and Jarl,[43] which yields:

$$f(\tau) = 1 - \left\{\frac{79\tau^{-1}}{140p} + \frac{474}{479}\left[\frac{1}{p} - 1\right]\left[\frac{\tau^3}{6} + \frac{\tau^9}{135} + \frac{\tau^{15}}{600}\right]\right\}/D \quad \tau < 1,$$
(Eq 8)

$$f(\tau) = -\left[\frac{\tau^{-5}}{10} + \frac{\tau^{-15}}{315} + \frac{\tau^{-25}}{1500}\right]/D \qquad \tau > 1,$$
(Eq 9)

$$D = \frac{518}{1125} + \frac{11692}{15975}\left(\frac{1}{p} - 1\right).$$
(Eq 10)

where p denotes the structure factor, which is the ratio of magnetic enthalpy in the paramagnetic state to the total magnetic enthalpy. For the BCC structure, the accepted value of p is 0.4, while $p = 0.28$ is used for the other structures.[42]

354

J. Phase Equilib. Diffus. (2021) 42:348–362

Table 5 Numerical details of the DFT calculations, including the k-meshes for the electronic and phonon properties, the supercell size and the number of atoms (sc atoms) for phonon calculations, and the cutoff energy (E_{cut} in eV)

Phase	k-mesh electron	Supercell size	sc atoms	k-mesh phonon	E_{cut}(eV)
αFe	$20 \times 20 \times 20$	$2 \times 2 \times 2$	16	$10 \times 10 \times 10$	600
αY	$14 \times 14 \times 9$	$3 \times 3 \times 3$	54	$4 \times 4 \times 4$	600
$Fe_{17}Y_2$	$5 \times 5 \times 5$	$1 \times 1 \times 1$	57	$5 \times 5 \times 5$	600
$Fe_{23}Y_6$	$4 \times 4 \times 4$	$1 \times 1 \times 1$	116	$4 \times 4 \times 4$	600
Fe_3Y	$10 \times 10 \times 2$	$2 \times 2 \times 1$	144	$4 \times 4 \times 1$	600
Fe_2Y	$8 \times 8 \times 8$	$2 \times 2 \times 2$	192	$3 \times 3 \times 3$	600

In this work, the Vienna ab−initio Simulation Package (VASP)[44, 45] code was applied to perform DFT calculations[46, 47]. Referring to the literature ?,[8–10] we used the generalized gradient approximation (GGA) approximation as parameterised by Perdew, Burke and Ernzerhof (PBE) for the exchange-correlation functional.[48] For the phonon calculation, the frozen phonon approach was applied with the help of the PHONOPY package.[45] Convergence tests were conducted in order to find out appropriate k-meshes and the cutoff energies, as listed in Table 5. We note that the Γ-centered k-meshes were used for the Brillouin zone integration. Additionally, the energy convergence criterion was set to be 10^{-6} eV/atom, and the corresponding tolerance of forces being 10^{-4} eV/Å during the ionic relaxations where the cell shape, cell volume and atomic positions are all optimized.

3.2 CALPHAD modeling

3.2.1 Pure elements

The Gibbs free energy of the pure element i (i = Fe and Y), referring to the enthalpy of its stable state at 298.15 K (H_i^{SER}), can be described as a function of temperature by:

$$^0G_i^\varphi(T) - H_i^{SER} = a + bT + cT\ln T + dT^2 + eT^{(-1)} + fT^3 + gT^7 + hT^{-9}$$

(Eq 11)

The coefficients a through h are taken from the SGTE database.[49]

3.2.2 Solution phases

The solution phases, Liquid, BCC_A2, FCC_A1 and HCP_A3 phases are described using the substitutional solution model, with the corresponding molar Gibbs free energy formulated as:

$$G_m^\varphi = x_{Fe}G_{Fe}^\varphi(T) + x_Y G_Y^\varphi(T) + RT(x_{Fe}\ln x_{Fe} + x_Y \ln x_Y) + G^{ex} + G^{mag}$$

(Eq 12)

where x_{Fe} and x_Y are the mole fraction of Fe and Y in the solution, respectively. Taken from the SGTE,[49] G_i^φ expresses the molar Gibbs free energy of pure Fe and Y in the structure φ at the given temperature. G^{ex} denotes the excess Gibbs energy of mixing, which measures the deviation of the actual solution from the ideal solution behaviour, modelled using a Redlich-Kister polynomial:[50]

$$G^{ex} = x_{Fe}x_Y \sum_{j=0}^n {}^{(j)}L_{Fe,Y}^\varphi (x_{Fe} - x_Y)^j.$$

(Eq 13)

The jth interaction parameters between Fe and Y are described by $^{(j)}L_{Fe,Y}^\varphi$, which is modelled in terms of a*+b*T.

3.2.3 Intermetallic Compounds

The alloys, $Fe_{17}Y_2$ and Fe_3Y, have already been reported as stoichiometric compounds based on the experimental phase diagram. Besides, it is clear that the solid solubility of $Fe_{23}Y_6$ and Fe_2Y are negligible. It is also noted that accurate DFT calculations on the hypothetical compounds, such as $Fe_{23}Y_6$ and Fe_2Y, would be a challenge because of the unknown crystal structures. Therefore, the compounds, $Fe_{23}Y_6$ and Fe_2Y were also treated as stoichiometric compounds in the current work.

Due to the lack of the heat capacity data, the Gibbs energies for the stoichiometric compounds in the traditional CALPHAD descriptions are described using the floating reference state (FRS), i.e., referring to the stable elements at different temperatures:

$$G_{Fe_mY_n} = \frac{m}{m+n} \cdot GHSER_{Fe} + \frac{n}{m+n} \cdot GHSER_Y + A^* + B^* \cdot T.$$

(Eq 14)

The parameters A^* and B^* correspond to the enthalpy and entropy of formation, often taken as constants for simplicity. Equation (11) implies that the heat capacity of the Fe-Y compounds follow the simple Neumann-Kopp rule in FRS. Consequently, an artificial kink appears on the heat capacity curve.[8, 9] Fortunately, such a shortcoming can be cured by using DFT calculated thermochemical data at finite temperatures as input parameters for the CALPHAD optimization, which delivers more physical meaning than using the polynomials as well. According to Ref. [8, 9], the Gibbs energy of an intermetallic phase above room temperature can be modelled as:

$$G_{Fe_mY_n} - H^{SER} = A + BT + CTlnT + DT^2 + ET^3 + FT^{-1} + G^{magn}_{Fe_mY_n}$$
(Eq 15)

where A and B are the parameters to be optimized, where their initial values can be obtained from the predicted enthalpy and entropy at 298 K based on DFT calculations. Coefficients C to F in Eq 15 are the related model parameters evaluated from the temperature-dependent heat capacity and hence the Gibbs energy. As suggested by Kubaschewski et al.,[51] C_p functions can be expressed as a polynomial:

$$C_p = -C - 2DT - 6ET^2 - 2FT^{-2}.$$
(Eq 16)

the thermodynamic optimization of the Fe-Y system was performed using the PARROT module of the Thermo-Calc software. Firstly, the Liquid interaction parameters L_0, L_1, and L_2 were modelled based on the experimental data of enthalpies of mixing.[23] Once the thermodynamic data of the Liquid were determined, the model parameters of the solid solution phases and the intermetallic phases were evaluated based on the phase equilibria data from Kubaschewski [13]. After several iterative optimizations, reasonable agreement between the calculated results and experimental or DFT results has been achieved. Table 6 lists the resulting thermodynamic parameters in this work.

Table 6 Thermodynamic parameters of the Fe-Y binary system.

Phase and model	Model parameters						Refs.
Liquid, (Fe,Y)$_1$	$L^{0,Liquid}_{Fe,Y} = -33172.2224 + 6.0006*T$						TW
	$L^{1,Liquid}_{Fe,Y} = -5055.64301$ to $5.39334840*T$						TW
	$L^{2,Liquid}_{Fe,Y} = 13849.1884 - 9.92512437*T$						TW
BCC_A2, (Fe,Y)$_1$: (Va)$_3$	$L^{0,BCC\_A2}_{Fe,Y} = 40000$						TW
	$^{298}T^{BCC\_A2}_{c,Fe:Va} = 1043$						49
	$^{298}\beta^{BCC\_A2}_{Fe:Va} = 2.20$						49
FCC_A1, (Fe,Y)$_1$:(Va)$_1$	$L^{0,FCC\_A1}_{Fe,Y} = 50000$						TW
	$^{298}T^{FCC\_A1}_{c,Fe:Va} = -201$						49
	$^{298}\beta^{FCC\_A1}_{Fe:Va} = -2.10$						49
HCP_A3, (Fe,Y)$_1$:(Va)$_{0.5}$	$^{0,HCP\_A3}_{Fe,Y} = 24000$						TW
Intermetallic compounds	$G^{Fe_mY_n} - H^{SER} = a + bT + cTlnT + dT^2 + eT^3 + fT^{-1} + G^{magn}_{Fe_mY_n}$						
	a	b	c	d	e	f	
Fe$_{17}$Y$_2$(298<T<1650)	-10000.000	149.41494	-27.893355	0.00192	$-8.342E-07$	157677.200	TW
	$^{298}T^{\alpha Fe_{17}Y_2}_{c,Fe:Y} = 328$						33
	$^{298}\beta^{\alpha Fe_{17}Y_2}_{Fe:Y} = 2.30$						TW
Fe$_{23}$Y$_6$(298<T<1623)	-10318.000	129.38000	-25.197900	-0.000812	$-4.640E-07$	93718.094	TW
	$^{298}T^{Fe_{23}Y_6}_{c,Fe:Y} = 484$						35
	$^{298}\beta^{Fe_{23}Y_6}_{Fe:Y} = 2.20$						TW
Fe$_3$Y(298<T<1621)	-10567.000	132.07651	-25.888740	-0.000241	$-3.430E-07$	88894.924	TW
	$^{298}T^{Fe_3Y}_{c,Fe:Y} = 569$						36
	$^{298}\beta^{Fe_3Y}_{Fe:Y} = 1.92$						TW
Fe$_2$Y(298<T<1401)	-10596.434	121.05000	-24.225300	-0.001842	$-2.400E-07$	49822.500	TW
	$^{298}T^{Fe_2Y}_{c,Fe:Y} = 545$						37
	$^{298}\beta^{Fe_2Y}_{Fe:Y} = 1.62$						TW

Gibbs energy is given in J per *mol-atom*, temperature (T) in Kelvin

T_c is the Curie temperature and β is the average magnetic moment per atom. (TW: this work. The parameters a and b are the optimized values, while c to f are the values derived based on DFT calculations)
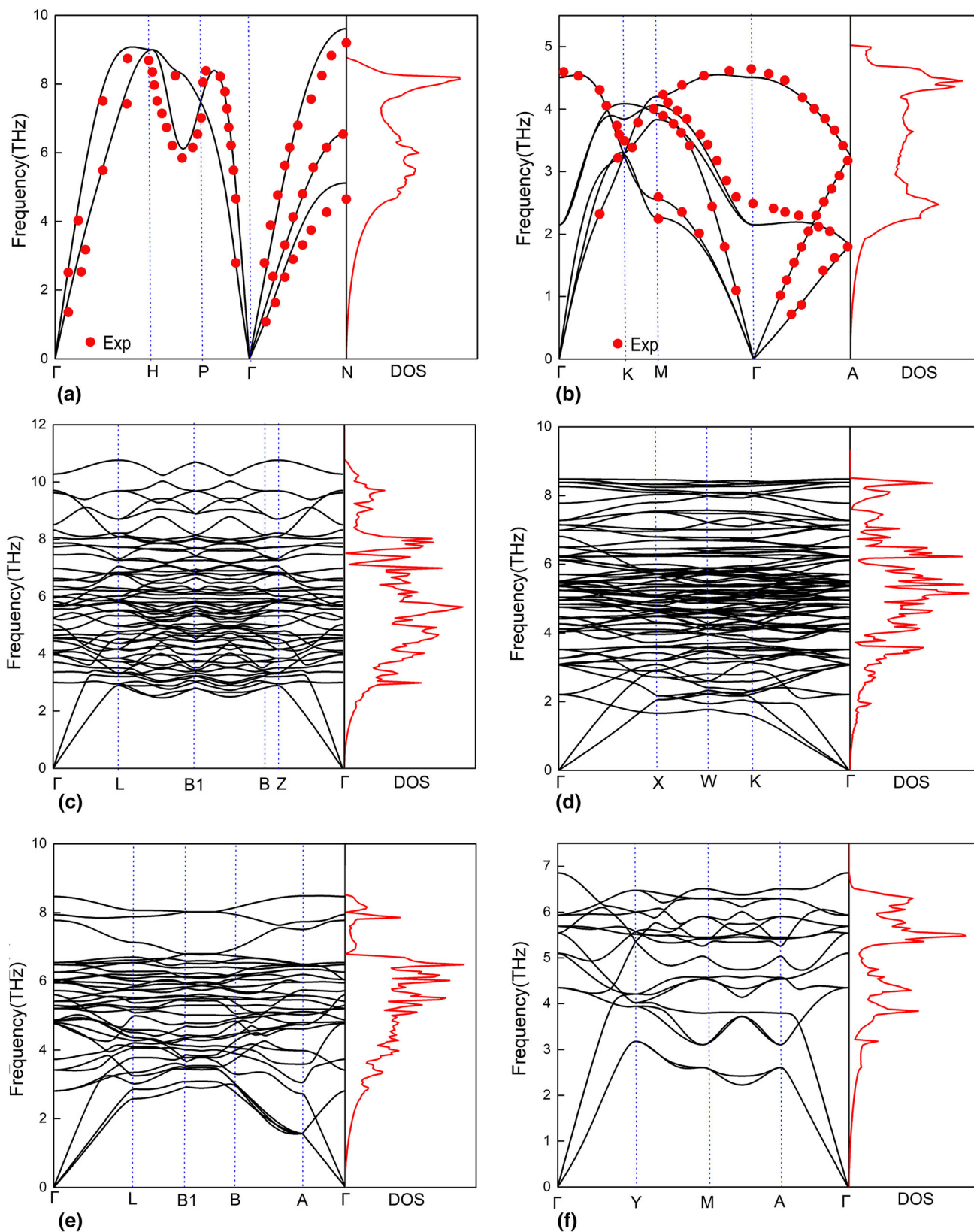
Fig. 2 Phonon dispersions and density of states (DOS) of the pure elements and intermetallic phases in the Fe-Y system: (a) BCC_Fe; (b) HCP_Y; (c) $Fe_{17}Y_{2-}$; (d) $Fe_{23}Y_6$; (e) Fe_3Y; (f) Fe_2Y. Available experimental data are included for comparison (solid circles)[52,53]

4 Results

4.1 Results from DFT Calculations

To benchmark our DFT calculations, the resulting crystallographic information of BCC_Fe, HCP_Y, $Fe_{17}Y_2$, $Fe_{23}Y_6$, Fe_3Y and Fe_2Y are listed in Table 1, in comparison with available experimental data. Obviously, the differences between the theoretical and experimental lattice constants are within 0.65 % for all the phases. Furthermore, the calculated phonon dispersions and PhDOS of such phases at the theoretical equilibrium volumes are shown in Fig. 2(a), (b), (c), (d), (e) and (f). To validate the calculations, as showed in Fig. 2(a) and (b), the phonon spectra of pure Fe and Y are compared with the experimental data,[52, 53] showing good agreement. Therefore, it is expected that the phonon properties of the Fe-Y intermetallic phases can also be accurately obtained based on DFT calculations. As shown in Fig. 2(c), (d), (e) and (f), imaginary phonon modes do not exist for all the compounds, indicating that they are all dynamically stable and the quasi-harmonic approximation (QHA) can be applied to get the thermodynamic properties.

The thermodynamic properties at finite temperatures are evaluated based on the Gibbs free energies as specified in Eq 1. Figure 3 shows the resulting heat capacity of the pure BCC_Fe and HCP_Y in comparison with the available experimental data,54–57 previous calculations[10] and SGTE.[49] For BCC_Fe, the magnetic contribution to the heat capacity is evaluated following the theory of Hillert and Jarl [43]:

$$Cp_{mag} = Rln(\beta^{\varphi} + 1)c(\tau). \tag{Eq 17}$$

As shown in Fig. 3(a), it is found that the theoretical results agree well with the experimental measurements[54] and SGTE.[49] Regarding HCP_Y, good agreement with Zacher's [10] results is obtained. Additionally, the resulting C_p is consistent with experiments[55] as well as SGTE[49] at low temperature, while it is slightly underestimated at high temperatures. This may be due to the anharmonic effects which are more significant at high temperatures. The calculated heat capacity of the $Fe_{17}Y_2$, $Fe_{23}Y_6$, Fe_3Y and Fe_2Y at finite temperatures are shown in Fig. 4(a) and (b), with the magnetic heat capacity evaluated using Eq 17.[43]

The enthalpies of formation of the intermetallic compounds at 0 K can be obtained by:

$$\Delta_f H^{Fe_mY_n} = H^{Fe_mY_n} - \frac{m}{m+n}H^{bcc}_{Fe} - \frac{n}{m+n}H^{hcp}_Y \tag{Eq 18}$$

where $H^{Fe_mY_n}$, H^{bcc}_{Fe} and H^{hcp}_Y are the calculated enthalpy per atom for Fe_mY_n, BCC_Fe and HCP_Y, respectively. As listed in Table 3, such enthalpies of formation are also consistent with previously reported results,[29] OQMD[31] and Materials Project.[30]

4.2 Result from the Thermodynamic Calculation

The assessed thermodynamic parameters by using the present set of model parameters are listed in Table 6. As shown in Fig. 5, the enthalpy of mixing for the liquid phase calculated at 1873 K are in good agreement with the experiments.[23] The calculated curve had a minimum value of − 8.23 kJ/mol at the composition of 47 at.% Y, perfectly matching the experimental value (− 8.44 kJ/mol). It is also evident that the calculated results obtained in this work reproduce well the experimental data, with significant improvements compared to the previous work.[5–7]

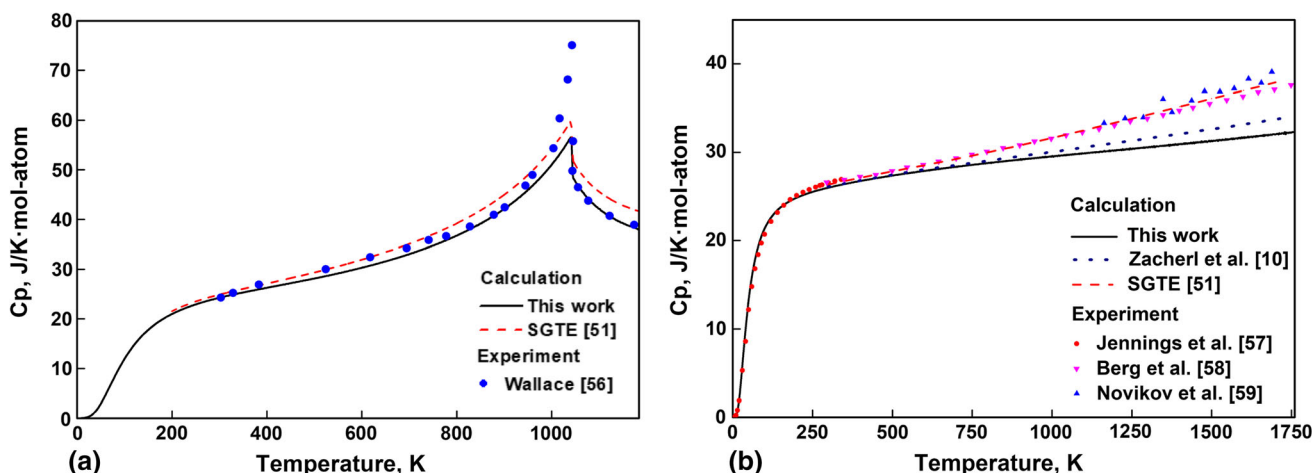Along with the available experimental data,[24] Fig. 6 shows the obtained activities of Fe and Y, in comparison

Fig. 3 Heat capacity of pure Fe and Y from DFT calculations in comparison with the experiment data,[54–57] previous work[10] and SGTE.[49] (a) Pure Fe; (b) Y
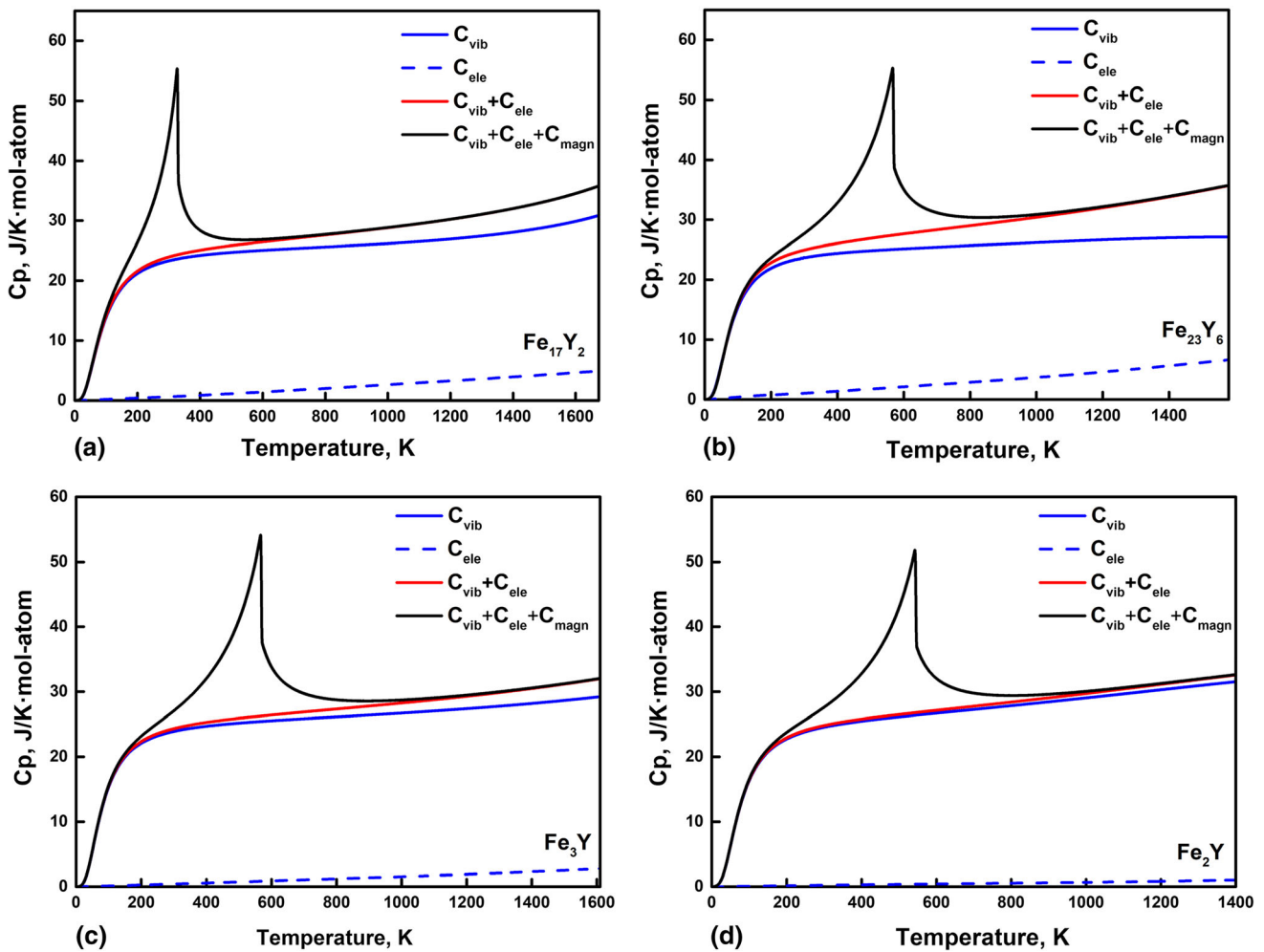
Fig. 4 Heat capacity of the intermetallic compounds in the Fe-Y system from DFT calculations. (a) $Fe_{17}Y_2$; (b) $Fe_{23}Y_6$; (c) Fe_3Y; (d) Fe_2Y
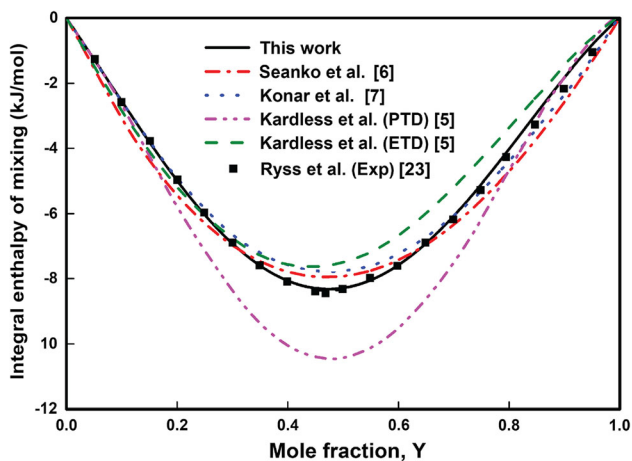

Fig. 5 Calculated integral enthalpies of mixing of the Fe-Y liquid at 1873 K with experiment data[23] and other optimized result[5–7]

with the reported results.[6] The calculated activities of Fe are in good agreement with the experimental results at both temperatures, though more positive results have been

obtained in the Y-rich region at 1473 K. Regarding the activities of Y, however, more positive values are obtained in the Liquid region. According to the work of Nagai et al.,[24] the activities of Y could be underestimated substantially because of the high oxygen contamination of Y. Similarly, the calculated activity of Fe and Y are acceptable, which are improved in comparison with the previous reports.[5–7]

The enthalpy of formation of the Fe-Y intermetallic phases at 298 K from the current CALPHAD modeling and DFT calculations are shown in Table 3 and Fig. 7, along with the previous CALPHAD modeling results.[5, 6] The enthalpy of formation of Fe_2Y and Fe_3Y at 298 K are − 6.412 and − 6.374 kJ/mol-atom, respectively, consistent with the DFT results (− 5.92 kJ/mol-atom for Fe_2Y and − 6.06 kJ/mol-atom for Fe_3Y). The enthalpy of formation of $Fe_{17}Y_2$ at 298 K (− 2.287 kJ/mol-atom) is also close to the values obtained by our DFT calculation (− 1.04 kJ/mol-atom). For $Fe_{23}Y_6$, the result is a bit less than the DFT values. Nevertheless, our present calculations
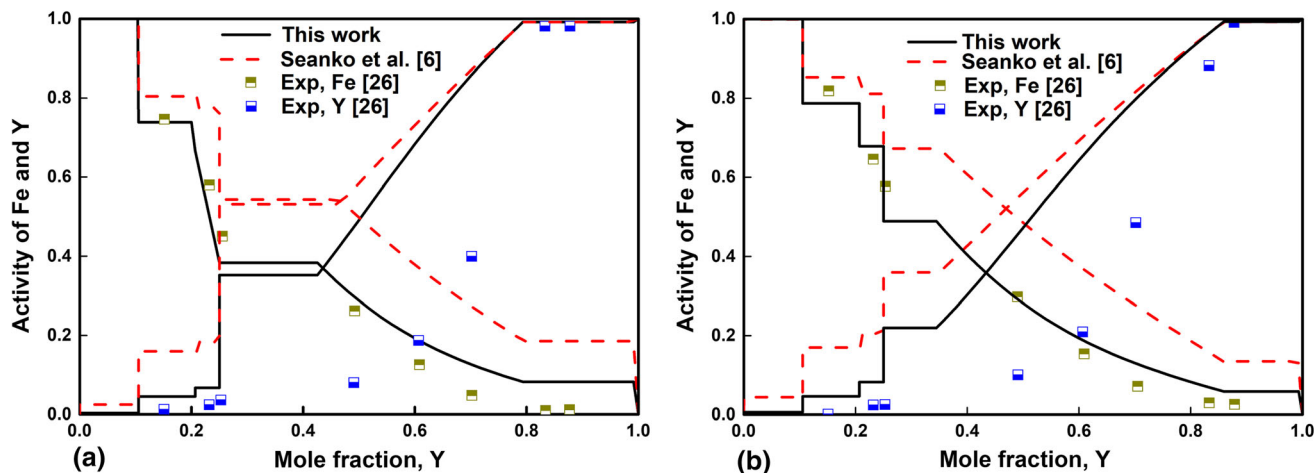
Fig. 6 Calculated activity of Fe and Y compared with experiment data[24] and previous result.[6] (a) 1473 K; (b) 1573 K
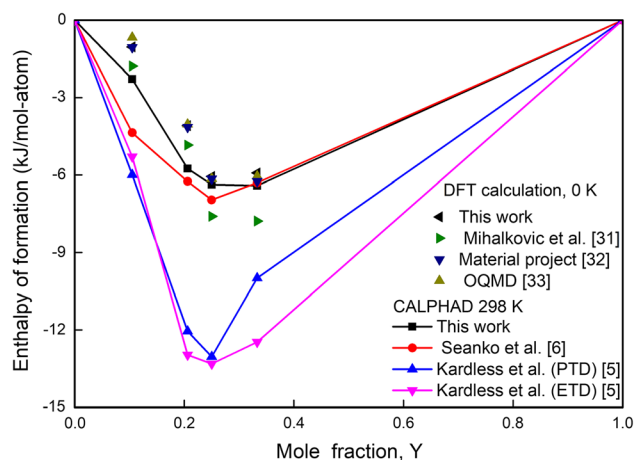

Fig. 7 Enthalpies of formation of the intermetallic compounds in the Fe-Y system at 0 K from DFT calculations[29–31] are compared with CALPHAD-assessed result at 298 K in this work and previous result[5, 6]

are more consistent with the DFT results in comparing to the previous work.[5, 6] In this regard, it suggests that the DFT calculations can provide reliable starting values for CALPHAD-optimization.

Comparing the CALPHAD-optimized enthalpy of formation in this work with that in previous work,[5, 6] it is observed that the assessed data in our work are in better agreement with the work of Seanko et al.,[6] whereas more positive than the results of Kardellass et al.[5] This is because when optimizing the Fe-Y system, Seanko et al.[6] considered the DFT results of Mihalkovivc et al.,[29] while completely empirical calculations based on traditionally thermodynamic models were done by Kardellass et al.[5]

Furthermore, the calculated enthalpies of formation of the four compounds at 973 K in our work are listed in Table 3 as well, in comparison with the experimental data of Subramanian and Smith[28] and previous assessed

results.[5, 6] The calculated enthalpies of formation are in good agreement with the experiment values, except for Fe_3Y with a slight overestimation (e.g., a deviation of 1.66 kJ/mol). Comparing with the previous assessments,[5–7] our results are in better agreement with the work of Seanko et al.,[6] while there is a noticeable deviation from the results of Kardellass et al.[5] As discussed above, this is because the thermal properties were not considered during assessment in Kardellass' results.[5]

The calculated Fe-Y phase diagram is presented in Fig. 8 along with the experimental data of Kubaschewski[13]. The enlarged part focuses on the phase relationships involving the $Fe_{17}Y_2$, $Fe_{23}Y_6$ and Fe_3Y phase (Fig. 8b). The comparison of the calculated temperatures and compositions of invariant reactions with experimental data by Kubaschewski[13] as well as results from previous thermodynamic assessments[5–7] are listed in Table 2. Obviously, good agreement between the optimized and experimental data on the phase relations is achieved. The peritectic reaction, i.e., Liquid + Fe_3Y → Fe_2Y is the most accurate calculation, where the calculated value is 1416 K consistent with the experimental data between 1373 K and 1423 K. The obtained eutectic reaction temperature L → γ Fe + $Fe_{17}Y_2$ at 1636 K in our CALPHAD modeling is also reasonable comparing with the experimentally measured value (1623 ± 25 K). Additionally, all the invariable reactions involving the terminal solid solution are acceptable by comparing with the experiments. Furthermore, the calculated congruent-melting point of $Fe_{17}Y_2$ (1650 K) from the current thermodynamic model is within the experimental temperature range from 1648 to 1698 K. Since there is no critical evidence of congruent melting for $Fe_{23}Y_6$ and Fe_3Y, their congruent temperature, i.e., 1622 K and 1621 K are calculated based on our DFT results and involved eutectic reactions. Similarly, the temperatures of the two eutectic reactions, Liquid → $Fe_{17}Y_2$ + $Fe_{23}Y_6$ and
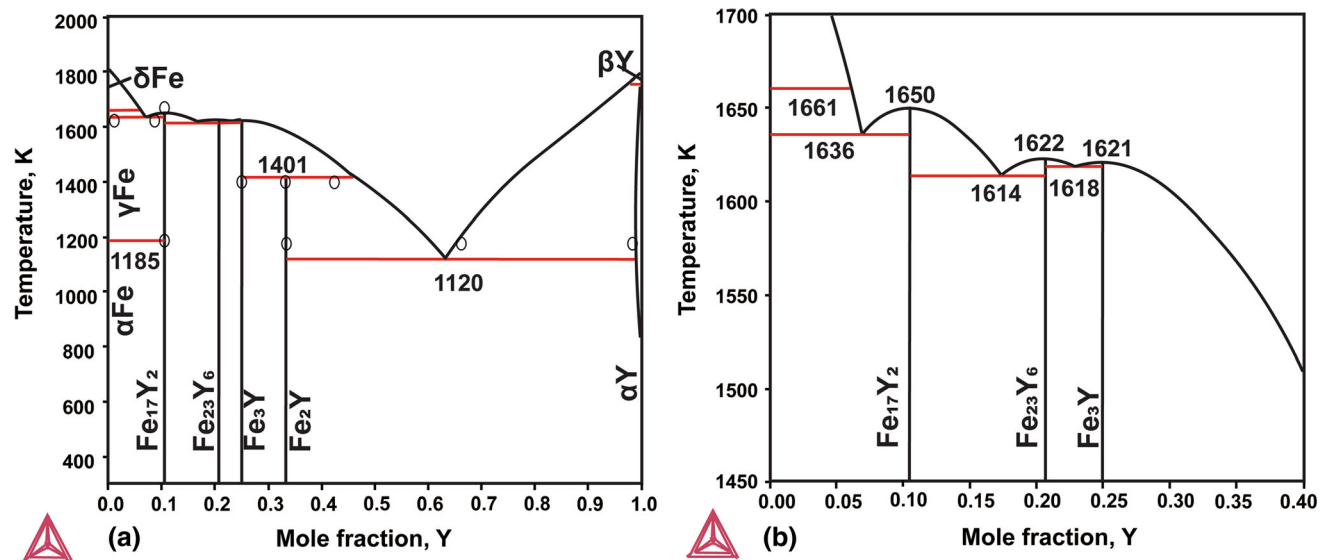
Fig. 8 The calculated Fe-Y phase diagram based on present thermodynamic modelling, in comparison with the experiment data (open circle).[13] (a) Fe-Y phase diagram on the entire composition range; (b) enlarged part of the Fe-Y phase diagram highlighting the phase relationship of $Fe_{17}Y_2$, $Fe_{23}Y_6$ and Fe_3Y

Liquid $\rightarrow$ $Fe_{23}Y_6$ + Fe_3Y are calculated to be 1613 K and 1619 K, respectively, which are close to the results of Kardellass et al.[5] and Seanko et al.[6]. In fact, the phase relationship involved in this part has not been well determined and further experiments are required to obtain a perfect solution.

5 Conclusions

The thermodynamic properties and phase equilibria of the Fe-Y binary system have been investigated, by combining DFT calculations and CALPHAD assessment. The quasi-harmonic phonon calculations have been performed to evaluated the phonon spectra for the intermetallic $Fe_{17}Y_2$, $Fe_{23}Y_6$, Fe_3Y and Fe_2Y phases, and to evaluate their finite-temperature thermodynamic properties together with the electronic and magnetic contributions to the Gibbs free energy. The resulting Gibbs free energy and heat capacity provide reliable input thermochemical values for the thermodynamic modelling. A complete set of self-consistent thermodynamic parameters are obtained via the CALPHAD method based on the available experimental data and DFT calculations. The optimized thermal properties of Liquid are in better agreement with the experiments than previous assessments and the optimized Fe-Y phase diagram has been improved as more physical meaning is introduced in the Gibbs free energy parameterizations.

References

1. O. Gutfleisch, M.A. Willard, E. Brück, C.H. Chen, S.G. Sankar, J. Ping Liu, Magnetic Materials and Devices for the 21st Century: Stronger, Lighter, and more Energy Efficient. Adv. Mater. **23**(7), 821–842 (2011)

2. M. Sagawa, S. Fujimura, N. Togawa, H. Yamamoto, Y. Matsuura, New Material for Permanent Magnets on a Base of Nd and Fe. J. Appl. Phys. **55**(6), 2083–2087 (1984)

3. X. Fan, G. Ding, K. Chen, S. Guo, C. You, R. Chen, D. Lee, A. Yan, Whole Process Metallurgical Behavior of the High-Abundance Rare-Earth Elements LRE (La, Ce and Y) and the Magnetic Performance of $Nd_{0.75}LRE_{0.25}$-Fe-B Sintered Magnets. Acta Mater. **154**, 343–354 (2018)

4. B. Peng, J. Jin, Y. Liu, Z. Zhang, M. Yan, Effects of (Nd, Pr)-Hx Addition on the Coercivity of Nd-Ce-Y-Fe-B Sintered Magnet. J. Alloy. Compd. **772**, 656–662 (2019)

5. S. Kardellass, C. Servant, N. Selhaoui, A. Iddaoudi, M. Ait Amar, L. Bouirden, A Thermodynamic Assessment of the Iron-Yttrium System. J. Alloy. Compd. **583**, 598–606 (2014)

6. I. Saenko, O. Fabrichnaya, A. Udovsky, New Thermodynamic Assessment of the Fe-Y System. J. Phase Equilib. Diff. **38**(5), 684–699 (2017)

7. B. Konar, J. Kim, I.-H. Jung, Critical Systematic Evaluation and Thermodynamic Optimization of the Fe-RE system: RE= Gd, Tb, Dy, Ho, Er, Tm, Lu, and Y. J. Phase Equilib. Diff. **38**(4), 509–542 (2017)

8. M.L. Song, H.K. Singh, H. Zhang, R. Schmid-Fetzer, Phase Equilibria of the Zn-Ti System: Experiments, First-Principles

Calculations and Calphad Assessment. Calphad **64**, 213–224 (2019)

9. J.H. Yong, Y. Wang, S.A. Firdosy, K.E. Star, P.F. Jean, V.A. Ravi, K.L. Zi, First-Principles Calculations and Thermodynamic Modeling of the Yb-Ni Binary System. Calphad **59**, 207–217 (2017)

10. C. Zacherl, J. Saal, Y. Wang, Z.K. Liu, First-Principles Calculations and Thermodynamic Modeling of the Re-Y System with Extension to the Ni-Re-Y System. Intermetallics **18**(12), 2412–2418 (2010)

11. R.D. Domagala, J.J. Rausch, D.W. Levinson, Y-Fe, Y-Ni and Y-Cu Systems. Trans. ASM **53**, 139–155 (1961)

12. K.A. Gschneidner, *Rare earth alloys* (D. Van Nostrand Co. Inc., Princeton, 1961), p. 247

13. O. Kubuschewski, *Iron-yttrium. Iron-binary phase diagrams* (Springer, New York, 1982), pp. 168–170

14. W. Zhang, G. Liu, K. Han, The Fe-Y (Iron-Yttrium) System. J. Phase Equilib. **13**(3), 304–308 (1992)

15. K.H.J. Buschow, The Crystal Structures of the Rare-Earth Compounds of the form R_2Ni_{17}, R_2Co_{17} and R_2Fe_{17}. J. Less Common Met. **11**(3), 204–208 (1966)

16. D.R. Wilburn, W.A. Bassett, Hydrostatic Compression of Iron and Related Compounds; An Overview. Am. Miner. **63**(5–6), 591–596 (1978)

17. Yu. Jun, X. Lin, J. Wang, J. Chen, W. Huang, First-Principles Study of the Relaxation and Energy of bcc-Fe, fcc-Fe and AISI-304 Stainless Steel Surfaces. Appl. Surf. Sci. **255**(22), 9032–9039 (2009)

18. M. Braun and R. Kohlhaas, Die spezifische wärme von Eisen, Kobalt und Nickel im bereich hoher temperaturen. physica status solidi (b) **12**(1), 429–444 (1965)

19. Z.S. Basinski, W. Hume-Rothery, A.L. Sutton, The Lattice Expansion of Iron. Proc. R. Soc. Lond. A **229**(1179), 459–467 (1955)

20. D.S. Evans, G.V. Baynor, Lattice Spacings in Thorium-Yttrium Alloys. J. Nucl. Mater. **2**(3), 209–215 (1960)

21. P. Villars, L.D. Calvert, *Pearson's Handbook of Crystallographic Data for Intermediate Phases* (American Society of Metals, Cleveland, 1985)

22. W. Zhang, W. Zhang, Collapse of the Magnetic Moment Under Pressure of AFe_2 (A= Y, Zr, Lu and Hf) in the Cubic Laves Phase. J. Magn. Magn. Mater. **404**, 83–90 (2016)

23. G.M. Ryss, A.I. Stroganov, Y.O. Esin, P.V. Gel'd, Enthalpy of Formation of Iron-Yttrium Liquid Alloys. Zhurnal Fizicheskoj Khimii **50**(3), 771–772 (1976)

24. T.N. Woong, H. Han, M. Maeda, Thermodynamic Measurement of La-Fe and Y-Fe Alloys by Multi-knudsen Cell Mass Spectrometry. J. Alloy. Compd. **507**(1), 72–76 (2010)

25. H.H. Van Mal, K.H.J. Buschow, A.R. Miedema, Hydrogen Absorption of Rare-Earth (3d) Transition Intermetallic Compounds. J. Less-Common Met. **49**(1–2), 473–475 (1976)

26. A.R. Miedema, On the Heat of Formation of Solid Alloys. II. J. Less-Common Met. **46**(1), 67–83 (1976)

27. D. Gozzi, M. Iervolino, A. Latini, Thermodynamics of Fe-Rich Intermetallics Along the Rare Earth Series. J. Chem. Eng. Data **52**(6), 2350–2358 (2007)

28. P.R. Subramanian, J.F. Smith, Thermodynamics of Formation of Y-Fe Alloys. Calphad **8**(4), 295–305 (1984)

29. M. Mihalkovič, M. Widom, Ab Initio Calculations of Cohesive Energies of Fe-Based Glass-Forming Alloys. Phys. Rev. B **70**(14), 144107 (2004)

30. A. Jain, S.P. Ong, G. Hautier, W. Chen, W.D. Richards, S. Dacek, S. Cholia, D. Gunter, D. Skinner, G. Ceder, K.A. Persson, The Materials Project: A Materials Genome Approach to Accelerating Materials Innovation. APL Mater. **1**(1), 011002 (2013)

31. S. Kirklin, J.E. Saal, B. Meredig, A. Thompson, J.W. Doak, M. Aykol, S. Rühl, C. Wolverton, The Open Quantum Materials Database (OQMD): Assessing the Accuracy of DFT Formation Energies. npj Comput. Mater. **1**(1), 1–15 (2015)

32. K. Mandal, A. Yan, P. Kerschl, A. Handstein, O. Gutfleisch, K.H. Müller, The Study of Magnetocaloric Effect in R_2Fe_{17} (R= Y, Pr) Alloys. J. Phys. D Appl. Phys. **37**(19), 2628 (2004)

33. G.W. Yin, F. Yang, C. Chen, N. Tang, H. Pan, Q. Wang, Structure and Magnetic properties of $Y_2Fe_{17-x}Mn_x$ Compounds (x = 0–6). J. Alloy. Compd. **242**(1–2), 66–69 (1996)

34. R. Coehoorn, Calculated Electronic Structure and Magnetic Properties of Y-Fe Compounds. Phys. Rev. B **39**(18), 13072 (1989)

35. J.F. Herbst, J.J. Croat, Magnetization of R_6Fe_{23} Intermetallic Compounds: Molecular Field Theory Analysis. J. Appl. Phys. **55**(8), 3023–3027 (1984)

36. K.H.J. Buschow, Intermetallic Compounds of Rare-Earth and 3d Transition Metals. Rep. Prog. Phys. **40**(10), 1179 (1977)

37. K.H.J. Buschow, Crystal Structure and Magnetic Properties of $YFe_{2x}Al_{l2-2x}$ Compounds. J. Less Common Met. **40**(3), 361–363 (1975)

38. W. Zhen Min Du, J. Zhang, Z.Z. Yu, Thermodynamic Assessment of the Fe-Y System. Rare Met. (English Edition) (China) **16**(1), 52–58 (1997)

39. D.X. Lü, C.P. Guo, C.R. Li, D. Zhen Min, Thermodynamic Description of Fe-Y and Fe-Ni-Y Systems. Phys. Procedia **50**, 383–387 (2013)

40. S. Kardellass, C. Servant, N. Selhaoui, A. Iddaoudi, M. Ait Amari, and L. Bouirden. Thermodynamic Assessments of the Fe-Y and Ni-Sc Systems. in *MATEC Web of Conferences*, vol. 3, p. 01008. EDP Sciences (2013)

41. Y. Wang, Z.K. Liu, L.Q. Chen, Thermodynamic Properties of Al, Ni, NiAl, and Ni_3Al from First-Principles Calculations. Acta Mater. **52**(9), 2665–2671 (2004)

42. G. Inden. Approximate description of the configurational specific heat during a magnetic order-disorder transformation. in *Proceeding of the 5th project meeting CALPHAD*, vol. 3, pp. 4–1 (1976)

43. M. Hillert, M. Jarl, A Model for Alloying in Ferromagnetic Metals. Calphad **2**(3), 227–238 (1978)

44. G. Kresse, J. Furthmüller, Efficiency of Ab-Initio Total Energy Calculations for Metals and Semiconductors Using a Plane-Wave Basis Set. Comput. Mater. Sci. **6**(1), 15–50 (1996)

45. A. Togo, I. Tanaka, First Principles Phonon Calculations in Materials Science. Scripta Mater. **108**, 1–5 (2015)

46. P.E. Blöchl, Projector Augmented-Wave Method. Phys. Rev. B **50**(24), 17953 (1994)

47. G. Kresse, J. Furthmüller, Efficient Iterative Schemes for ab Initio Total-Energy Calculations Using a Plane-Wave Basis Set. Phys. Rev. B **54**(16), 11169–11186 (1996)

48. J.P. Perdew, K. Burke, M. Ernzerhof, Generalized Gradient Approximation Made Simple. Phys. Rev. Lett. **77**(18), 3865 (1996)

49. A.T. Dinsdale, SGTE Data for Pure Elements. Calphad **15**(4), 317–425 (1991)

50. O. Redlich, A.T. Kister, Algebraic Representation of Thermodynamic Properties and the Classification of Solutions. Ind. Eng. Chem. **40**(2), 345–348 (1948)

51. O. Kubaschewski, C.B. Alcock, P.J. Spencer, *Materials Thermochemistry*, 6th edn. (Pergamon Press, London, 1993)

52. B.N. Brockhouse, H.E. Abou-Helal, E.D. Hallman, Lattice Vibrations in Iron at 296 k. Solid State Commun. **5**(4), 211–216 (1967)

53. H.P. Sinha, J.C. Upadhyaya, Phonon Dispersion in Some HCP Transition Metals. Physica B+C **79**(4), 359–369 (1975)

362

J. Phase Equilib. Diffus. (2021) 42:348–362

54. D.C. Wallace, P.H. Sidles, G.C. Danielson, Specific Heat of High Purity Iron by a Pulse Heating Method. J. Appl. Phys. **31**(1), 168–176 (1960)

55. L.D. Jennings, R.E. Miller, F.H. Spedding, Lattice Heat Capacity of the Rare Earths. Heat Capacities of Yttrium and Lutetium from 15–350 k. J. Chem. Phys. **33**(6), 1849–1852 (1960)

56. J.R. Berg, F.H. Spedding, A.H. Daane, *The High Temperature Heat Contents and Related Thermodynamic Properties of Lanthanum, Praseodymium, Europium, Ytterbium, and Yttrium* (Ames Lab., Ames, Iowa, Technical Report, 1961)

57. I.I. Novikov, I.P. Mardykin, Specific Heats of Yttrium and Gadolinium at High Temperatures. Soviet Atomic Energy **37**(4), 1088–1090 (1974)